

## Fusion Well Below the Barrier

W. Reisdorf, F. Heßberger, K. Hildenbrand, S. Hofmann, J.V. Kratz, G. Münzenberg, K.-H. Schmidt,  
W.F.W. Schneider, K. Sümmerer, G. Wirth  
GSI Darmstadt

From recent experiments<sup>1,2,3</sup> it follows that fusion below the classical barrier cannot be described in terms of the conventional one-dimensional transmission models using any of the currently proposed conservative nucleus-nucleus potentials, despite an apparent success of these models to describe reasonably well fusion above the classical barrier<sup>4</sup>. As a general rule one tends to observe unexpectedly large cross sections below the barrier. More specifically, there is also some evidence that this cross section enhancement is dependent on the nature of the amalgamating nuclei. In a comparative study it was shown, first, that the apparent threshold lowering was larger for well deformed target nuclei (<sup>154</sup>Sm) than for spherical nuclei (<sup>144</sup>Sm) and, second, that the global effect was stronger if the projectile partner was heavier. Fusion studies of Cl and Ca with a series of Ni isotopes<sup>2</sup> also indicated that the threshold lowering, after removal of the  $A^{1/3}$  scaling, seemed to increase with increasing mass (softness) of the Ni isotopes. Recent, puzzling, observations<sup>3</sup> of fusion of the Ni+Ni system have been interpreted as due to the influence of valence nucleons on the fusion cross sections.

We have determined high precision fusion excitation functions for  $^{40}\text{Ar} + ^{112,116,122}\text{Sn}$  and made improved measurements for  $^{40}\text{Ar} + ^{144,148,154}\text{Sm}$ . From the comparison of these excitation functions we hope to separate more unambiguously the effects of static deformation, if any, than was previously possible since the various tin isotopes are all spherical in contrast to the samarium isotopes. The effects of the projectile mass (or the entrance channel asymmetry) on the threshold lowering will be studied in the near future in reactions of <sup>86</sup>Kr with various Ru and Ge isotopes.

The experimental method involves the combination of a velocity filter and activation methods for the measurement of evaporation residues and an ionization chamber for the measurement of fission cross sections. While being an independent method<sup>1</sup>, the activation method which involves off-line K x ray and gamma spectroscopy using catcher methods, also allows to calibrate the transmission of the, more sensitive, velocity filter. Figure 1 shows the decay curve of the K x rays from xn products in the reaction  $^{40}\text{Ar} + ^{122}\text{Sn}$  with a catcher exposed directly to the beam ('X3') and a catcher behind the velocity filter ('SHIP'). Measurements at the velocity filter consist in registering the signals from the evaporation residues implanted in a position sensitive solid state detector after having passed the filter and a two-detector time-of-flight system (thin carbon foils

with electrostatic deflection of the emitted electrons onto a large channel plate). Figure 2 shows in a time-of-flight versus energy diagram that the evaporation residues (ER) are well separated from the background of Ar projectiles despite the low fusion cross section (0.2 mb in the figure).

Evaluation is still in progress. Figure 3 shows preliminary data for  $^{40}\text{Ar} + ^{122}\text{Sn}$ . The fusion cross section has been measured over almost six orders of magnitude. The solid curve is a transmission calculation (WKB) using a proximity potential and assuming sphericity for both target and projectile. The threshold lowering relative to this calculation is quite striking.

<sup>1</sup>R.G. Stokstad et al., Z. Physik A295 (1980) 295

<sup>2</sup>B. Sikora et al., Phys. Rev. 20 (1979) 2219

<sup>3</sup>M. Beckerman et al., Phys. Rev. Lett. 45 (1980) 1472

<sup>4</sup>J.R. Birkelund et al., Phys. Rep. 56 (1979) 108

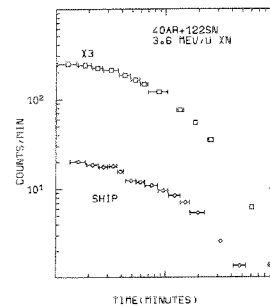


Figure 1

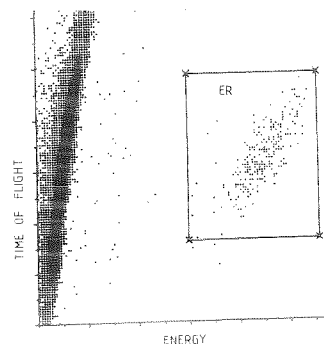


Figure 2

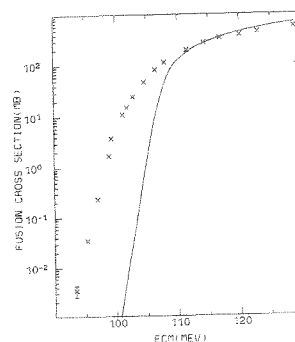


Figure 3

Sub-Coulomb Fission and Transfer in Collisions of  $^{208}\text{Pb}$  with  $^{238}\text{U}$ 

W. Brüche, H. Folger, B. Haefner, J.V. Kratz

GSI Darmstadt

G. Friedländer\*

Institut für Kernchemie, Universität Mainz

Off-line radiochemical measurements of cross sections for neutron stripping and pick-up processes and for fission were performed in the  $^{208}\text{Pb} + ^{238}\text{U}$  system at energies below the Coulomb barrier ( $0.74 \leq E/B \leq 0.90$ ). The fission products  $^{139}\text{Ba}$  and  $^{97}\text{Zr}$ , and the transfer products  $^{239}\text{U}$  and  $^{237}\text{U}$  were separated chemically from the irradiated targets. Details are given elsewhere.<sup>1</sup> Their activities were measured in a low-level  $\beta$ -proportional counter, and with shielded Ge(Li) detectors in absolutely calibrated counting positions.

As in a preceding experiment<sup>1</sup> with the systems  $^{129,132,136}\text{Xe} + ^{238}\text{U}$  some difficulty was encountered with oxygen contamination of the  $^{238}\text{U}$  targets. Even though prepared essentially oxygen-free the targets were found to get residual oxygen from the vacuum during bombardment. Previously, this had been detected via formation of  $^{133\text{m}}\text{Ba}$  and  $^{135\text{m}}\text{Ba}$  in transfer reactions with the Xe projectiles. Fission of  $^{238}\text{U}$  induced by neutrons being evaporated in these transfer reactions was monitored and corrected for, if detectable.<sup>1</sup> In the present experiments transfer reactions of the  $^{208}\text{Pb}$  projectile with  $^{16}\text{O}$  target impurities were found to directly produce a small but detectable amount of symmetric fission products resulting from sequential fission of Pb-like fragments as evidenced by formation of  $^{97}\text{Zr}$  in the bombardment of a  $\text{Bi}_2\text{O}_3$  target with  $^{208}\text{Pb}$ . The background of  $^{139}\text{Ba}$  activity produced simultaneously was negligible. Neutron-induced fission was not detectable. In agreement with these findings, in the bombardment of  $^{238}\text{U}$ -targets with  $^{208}\text{Pb}$ -ions we found  $^{97}\text{Zr}$  yields that were systematically higher than the  $^{139}\text{Ba}$  cross sections, indicating the presence of some oxygen in the target. (In low-energy uranium fission the cumulative yields of  $^{97}\text{Zr}$  and  $^{139}\text{Ba}$  are very nearly the same). Therefore, the fission cross sections shown in the figure are only based on the cumulative  $^{139}\text{Ba}$  yields with the assumption of a 6.5% fission yield for mass chain 139. Also shown are the cross sections for the neutron stripping and pick-up processes with  $^{238}\text{U}$ . The latter can be used to estimate in a semiquantitative way<sup>2</sup> the transfer-fission probabilities associated with these channels and with other transfer channels not observed experimentally. This is done on the basis of the  $(Q_{\text{gg}} - Q_{\text{opt}})$ -values representing the excitation energies in the residual nucleus at which transfer is favoured. Because Coulomb excitation occurs before and following transfer we have added an average excitation

energy of 3.5 MeV to the  $(Q_{\text{gg}} - Q_{\text{opt}})$ -value. The transfer probabilities are then obtained by assuming a Gaussian distribution of excitation energies around the mean value with a width of  $\text{FWHM} = 7$  MeV. Integration over all states with energies above  $B_f = 6$  MeV then yields the transfer-fission probabilities. If we take, for example, a fission probability  $P_f = 0.3$  for all states above  $B_f$  we obtain at  $E/B = 0.8$  a total transfer-fission probability of 0.05 mb, i.e. 10% of the observed fission cross section. At lower values of  $E/B$  this fraction is even smaller. In the figure the fission cross sections based on the  $^{139}\text{Ba}$  yields are compared with theoretical predictions<sup>3</sup> for Coulomb fission. For the lowest energies this indicates that we may have observed pure Coulomb fission.

\*Holder of an Alexander von Humboldt-Award, on leave from Brookhaven National Laboratory

<sup>1</sup>G. Franz et al., Z. Physik **A291**, 167 (1979)

<sup>2</sup>J.R. Leigh et al., Phys. Rev. Lett. **92**, 153 (1979)

<sup>3</sup>V. Oberacker et al., Phys. Rev. **C20**, 1453 (1979) and private communication

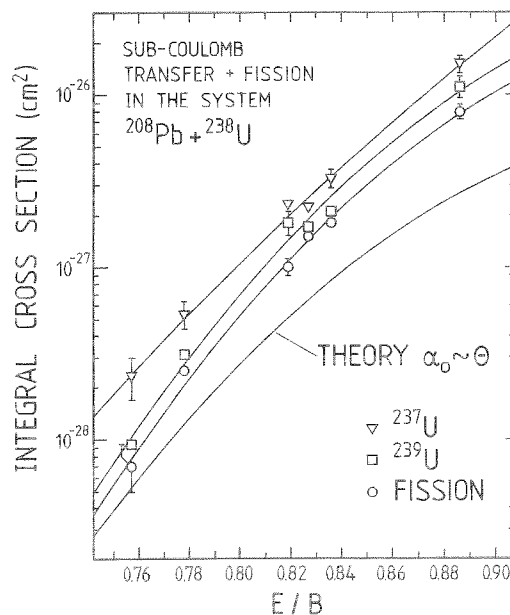


Fig. 1: Integral cross sections for formation of  $^{237}\text{U}$ ,  $^{239}\text{U}$ , and for fission in  $^{208}\text{Pb} + ^{238}\text{U}$  collisions as a function of the centre-of-mass energy  $E$  relative to the classical interaction barrier  $B$ . The solid lines are to guide the eye. The lowest solid line is the theoretical prediction for Coulomb fission (Ref. 3) for the moment of inertia  $\Theta$  being proportional to the deformation  $\alpha_0$ .

Influence of the Entrance Channel Mass Asymmetry on the Production of Cold Fermium Compound Nuclei

T. Sikkeland\* and H. Gäggeler  
GSI Darmstadt

No evidence has to far been found for the production of surviving superheavy elements (SHE) in heavy ion fusion reactions. At present it is not understood whether the failure is connected with entrance channel phenomena or with the instability of highly excited ( $E^* \geq 20$  MeV) SHE against prompt fission. In order to study the influence of the entrance channel on the compound nucleus formation,  $^{246}\text{Fm}$  was produced by different projectile-target combinations at energies near the interaction barrier. The isotope  $^{244}\text{Fm}$  from the 2n-evaporation channel was then detected as a probe for fusion at low excitation energies. This isotope was chosen since i) it is known to decay by spontaneous fission with a half-life of about 3 ms, ii) it has already been produced in a (HI,2n)-reaction ( $^{40}\text{Ar} + ^{206}\text{Pb}$ ), and iii) it can easily be detected with high efficiency ( $\approx 60\%$ ) using a rotating wheel system. Since the fusion barriers for different projectile-target combinations are unknown, relatively thick targets ( $\approx 3$  mg/cm<sup>2</sup>) were used in order to cover a broad energy range within the target [about 40 MeV (CM)]. The outgoing projectile energy behind the target was chosen to be the 2n-threshold energy. In the table are summarized the results obtained after two irradiations of Kr + Gd and Xe + Pd. Both experiments gave negative results leading only to cross section limits for the production of  $^{244}\text{Fm}$ . The maximum cross section  $\sigma_{\text{max}}$  was deduced from the mean value  $\bar{\sigma}$  in the thick target assuming a width of the 2n excitation function of 10 MeV (FWHM)<sup>1</sup>. In the nearly symmetric reactions between Kr + Gd and Xe + Pd, due to the Q-values of these reactions,  $^{246}\text{Fm}$  should be produced with an excitation as low as 30 and 24 MeV at the barrier, respectively, which should much favour low xn-channels. The very low cross section limit observed in our experiment can be expressed in terms of an extra push of kinetic energy  $\Delta E$  over the interaction barrier needed to make two nuclei fuse as proposed by Swiatecki<sup>2</sup>. The values for  $\Delta E$  extracted from our cross section limits for  $^{244}\text{Fm}$  are shown in the figure (squares) together with the value for the same nucleus being produced from  $^{40}\text{Ar} + ^{206}\text{Pb}$  (circle)<sup>1</sup>, and two recent results from  $^{86}\text{Kr} + ^{123}\text{Sb}$  and  $^{124}\text{Sn} + ^{94}\text{Zr}$  (crosses)<sup>3</sup> as a function of  $(Z^2/A)_{\text{eff}}$  defined as<sup>2</sup>

$$\frac{(Z^2)_{\text{eff}}}{A} = \frac{4 Z_1 Z_2}{A_1^{1/3} A_2^{1/3} (A_1^{1/3} + A_2^{1/3})}$$

Table

Reaction	Dose	Energy (lab.)	$\bar{\sigma}$	$\sigma_{\text{max}}$
$^{86}\text{Kr} + ^{160}\text{Gd}$ (3 mg/cm <sup>2</sup> )	$2.0 \times 10^{16}$	409 MeV	$\leq 8 \times 10^{-35}$ cm <sup>2</sup>	$\leq 3 \times 10^{-34}$ cm <sup>2</sup>
$^{136}\text{Xe} + ^{110}\text{Pd}$ (2.5 mg/cm <sup>2</sup> )	$2.6 \times 10^{16}$	680 MeV	$\leq 4.5 \times 10^{-35}$ cm <sup>2</sup>	$\leq 2 \times 10^{-34}$ cm <sup>2</sup>

Also shown is a theoretical prediction of  $\Delta E$  from Ref. 2 (solid line). These results indicate that the extra push starts to increase the fusion barrier relative to the barrier as calculated with the proximity theory at higher values of  $(Z^2/A)_{\text{eff}}$  (about 37 - 39) as compared to the theoretical value from Ref. 2 ( $(Z^2/A)_{\text{crit}} = 26 - 27$ ).

- /1/ H. Gäggeler et al., Z. Physik A289, 415 (1979)  
/2/ W. J. Swiatecki, LBL report 10911 (1980)  
/3/ K. H. Schmidt et al., Contr. IXth. Workshop Hirschegg, Austria (1981)

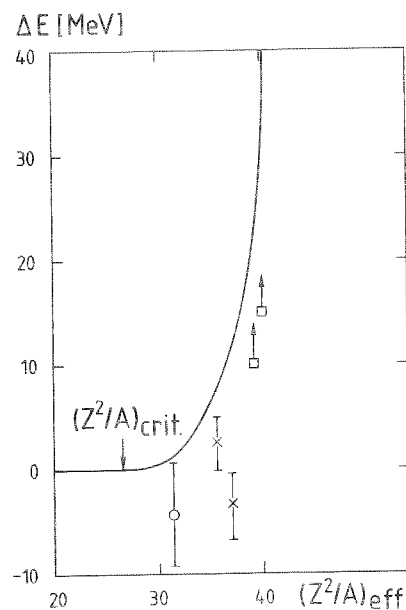


Figure 1: Differences between measured and calculated fusion barriers versus  $(Z^2/A)_{\text{eff}}$ . The effective nuclear potential was expressed by the proximity potential. The symbols are explained in the text.

Nucleon exchanges in damped collisions of  $^{208}\text{Pb} + ^{74}\text{Ge}$  and  $^{86}\text{Kr} + ^{197}\text{Au}$

G. Grégoire, R. Lucas, C. Mazur, C. Ngô, J. Poitou, M. Ribrag, CEN Saclay

U. Lynen, MPI Heidelberg

A. Gobbi, J.V. Kratz, A. Olmi, H. Sann, G. Wirth, GSI Darmstadt

We have investigated the neutron excess relaxation in deep inelastic collisions of  $^{208}\text{Pb}$  with  $^{74}\text{Ge}$  at 7.5 MeV/u and  $^{86}\text{Kr}$  with  $^{197}\text{Au}$  at 6.5 MeV/u.

As in the Kr + Mo<sup>1</sup> experiment we used a large ionization chamber of 22° acceptance angle at 60° from the beam direction for Pb + Ge ( $\theta_{gr} = 62^\circ$ ) and at 46° for Kr + Au ( $\theta_{gr} = 52^\circ$ ) measuring  $\Delta E$ , E and the scattering angle. The Z resolution was 0.7 and 0.8 charge units around the Ge and Kr respectively. A mass identification was also performed by a time of flight measurement using the microstructure (when it was narrow enough) of the Unilac. The mass resolution obtained was of 2 to 2.5 mass units.

For these two systems we calculated the mean values  $\langle A \rangle$ ,  $\langle Z \rangle$  as well as the variances  $\sigma_A^2$  and  $\sigma_Z^2$  and the correlation coefficients  $\rho(A, Z)$  and  $\rho(N, Z)$  of the mass and charge distributions as a function of the excitation energy. For both systems and for small energy damping the mass variances have a finite value while  $\sigma_Z^2$  is surprisingly small (fig. 1). The ratio  $\sigma_A^2/\sigma_Z^2$  is rather large up to 25 MeV for Kr on Au and 40 MeV for Pb on Ge. For increasing energy losses this ratio decreases to a value close to  $(\langle A \rangle / \langle Z \rangle)^2$  for Kr on Au but higher than  $(\langle A \rangle / \langle Z \rangle)^2$  for Pb on Ge ( $\sigma_A^2/\sigma_Z^2 \rightarrow 11$ ,  $(\langle A \rangle / \langle Z \rangle)^2 = 5.8$ ). According to Rudolf et al.<sup>2</sup> the saturation of  $\sigma_A^2/\sigma_Z^2$  at a value of about  $(\langle A \rangle / \langle Z \rangle)^2$  is representative of a high correlation between neutron and proton exchanges, and indeed we find that the full correlation ( $\rho(N, Z) = 1$ ), is reached for about the same loss of energy than the saturation of  $\sigma_A^2/\sigma_Z^2$ . Initially (at low excitation energy) neutrons are preferentially transferred while the Coulomb force hinders proton transfer. Similar results have been found in other experiments<sup>3</sup>.

A contour plot in the N, Z plane of the potential energy surface (PES) using shell corrected liquid drop ground state masses is shown in fig. 2 for the two systems. Also shown are the centroids of the measured N-Z distributions starting from the elastic events in a sequence of energy bins 10 MeV wide. Contrary to most of the so far studied systems the measured behaviour can not be explained by a static potential energy surface; account has to be taken of the variation of the energy surface with angular momentum and distance of closest approach (or deformations).

The widths of the Z distributions for fixed mass asymmetry as a function of the loss of energy have also been found<sup>4</sup> to have an intermediate behaviour between the previously studied Kr + Mo<sup>1</sup> and Xe + Au<sup>3</sup>. Evaporation calculations<sup>5</sup> indicate dominant neutron evaporation thus confirming the obtained  $\sigma_Z^2$ . Dynamical calculations using the code of

Grégoire et al.<sup>6</sup> are underway.

<sup>1</sup>M. Berlinger et al., Z. Phys. A291(1979)133

<sup>2</sup>G. Rudolf et al., Nucl. Phys. A330(1979)243

<sup>3</sup>J.V. Kratz et al., Nucl. Phys. in press  
Z. Phys. A296(1980)141

<sup>4</sup>A. Gobbi et al., Annual Report Saclay 1980

<sup>5</sup>(Code Pace) Y. Eyal, A. Gavron, unpublished

<sup>6</sup>C. Gregoire et al., Phys. Letters, to be published

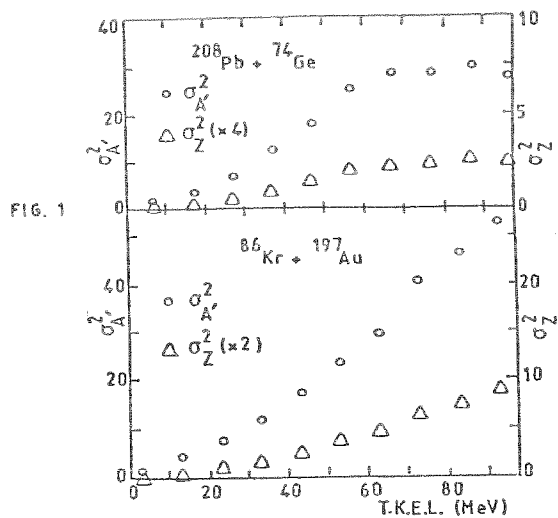


FIG. 1

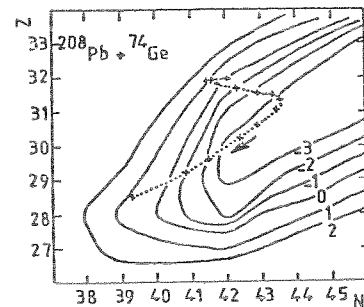
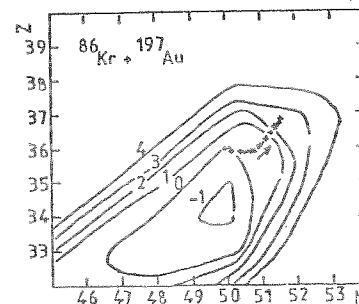


FIG. 2



On the reconstruction of primary mass and charge distributions  
from measured secondary quantities in damped heavy-ion collisions

J. Poitou<sup>†</sup>, J. V. Kratz, G. Wirth  
GSI Darmstadt

R. Lucas

Département de Physique Nucléaire, CEN Saclay, France

The high-resolution measurement of mass and charge distributions as a function of the dissipated energy in damped heavy-ion collisions is of great current interest. However, the interpretation of such data is difficult because many of the primary properties are modified during the deexcitation of the excited primary fragments by evaporation processes. If neutron-evaporation alone has to be considered, the calculation of a primary mass number  $A'$  associated with the measured secondary mass  $A$  requires precise knowledge of the excitation energy. However, this quantity can only be determined from the measured kinetic energy  $E_k$  if  $A'$  is known. This problem can only be solved for mean values in an iterative way with the additional assumption of a division of the total excitation energy in strict proportion to the fragment masses. Again, the latter assumption is only justified on the average. At present, it is completely unknown what variances occur in the division of the total excitation energy between the two fragments. Thus, the usual corrections of post-neutron emission yield distributions for particle evaporation can strictly determine only mean values for the primary distributions and it may be difficult to interpret second moments resulting from conventional correction procedures.

We have developed a correction procedure<sup>1</sup> which takes explicitly into account the fact that the observed secondary distribution is a convolution of the primary distribution by an excitation energy distribution. The essential piece of experimental information that is being used in this reconstruction is the (linear) dependence of the average excitation energy  $\langle E \rangle_{A,Z}$  associated with the formation of post-neutron emission isotopes of a given  $Z$  on the post-neutron emission mass number  $A$ . The resulting variance of the excitation energy distribution then contains also the eventual contribution resulting from fluctuations in the division of the total excitation energy between the two fragments.

Starting from i) the experimentally determined mean values for the post-neutron emission quantities  $\langle E \rangle_{A,Z}$  and  $\langle A \rangle_Z$ , ii) the variance of the post-neutron emission isotope distribution  $\sigma^2(A;Z)$ , and iii) the element yield  $P(Z)$ , for each element  $Z$ , the procedure derives a complete mathematical surface describing the primary distribution  $P(E, A', Z)$ .

Uncertainties in the deduced primary quantities are derived by a Monte Carlo calculation from the experimental

uncertainties and from estimated systematic uncertainties associated with the evaporation simulations. It is then possible to calculate numerically from  $P(E, A', Z)$  any zeroth, first or second moment of one variable conditioned by any of the remaining variables as well as their mutual correlations.

As an example we show in Fig.1 the integral variances  $\sigma^2(A';E)$  and  $\sigma^2(Z;E)$ , the ratio of these variances, and the correlation coefficients  $\rho(A', Z; E)$  and  $\rho(N, Z; E)$  for the  $^{132}\text{Xe} + ^{197}\text{Au}$  reaction at 900 MeV. A detailed discussion of these results is given elsewhere.<sup>2</sup>

<sup>†</sup>On leave of absence from DPh-N/MF, CEN Saclay, France.

<sup>1</sup>J. Poitou et al., GSI-Preprint 80-21 (1980), Nucl. Instr. Meth., in press

<sup>2</sup>J.V. Kratz et al., GSI-Preprint 80-22 (1980), Nucl. Phys. A, in press

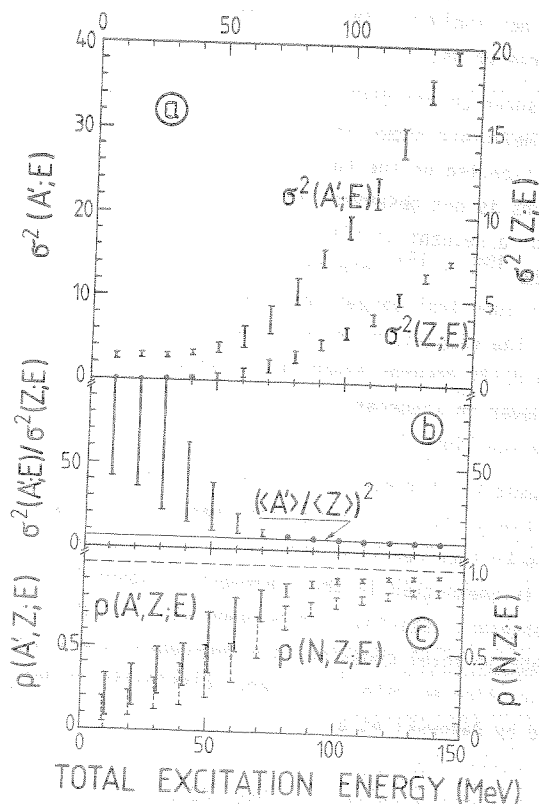


Fig. 1: Moments of the reconstructed primary mass and charge distributions in the reaction of 900 MeV  $^{132}\text{Xe}$ -ions with  $^{197}\text{Au}$  as a function of the total excitation energy (from Ref. 2). (a) Integral particle number variances, (b) ratio of the integral mass and charge variances, and (c) correlation coefficients.

Heavy actinide cross sections in the  $^{238}\text{U} + ^{248}\text{Cm}$  reaction

M. Schädel, W. Brüche, H. Gäggeler, J. V. Kratz, K. Sümmerer, G. Wirth  
GSI Darmstadt

G. Herrmann<sup>†</sup>, R. Stakemann, N. Trautmann  
Institut für Kernchemie, Universität Mainz

J. M. Nitschke  
Lawrence Berkeley Laboratory

E. K. Hulet, R. W. Lougheed  
Lawrence Livermore National Laboratory

R. L. Hahn, R. L. Ferguson  
Oak Ridge National Laboratory

In order to investigate the potential of the  $^{238}\text{U} + ^{248}\text{Cm}$  reaction for the transfer of many nucleons together with little excitation energy cross sections for the production of heavy actinide isotopes were determined by radiochemical techniques. Experimental details are already described in Ref. 1. The measured cross sections for the production of  $^{98}\text{Cf}$ ,  $^{99}\text{Es}$ ,  $^{100}\text{Fm}$  and  $^{101}\text{Md}$  isotopes in the bombardment of thick  $^{248}\text{Cm}$  targets with 7.4 MeV/u  $^{238}\text{U}$ -ions ( $1.18 \geq E/B \geq .96$ ) are shown in Fig. 1. Simultaneously, evaporation residues from the much less fissile fragments  $^{84}\text{Po}$  and  $^{85}\text{At}$  were identified and were found to have about the same cross sections as determined previously<sup>2</sup> in the  $^{238}\text{U} + ^{238}\text{U}$  reaction in the same range of energies E/B, indicating that the primary, pre-fission yield distribution has the same width in both reactions. Then, if we shift the reconstructed primary distribution of target-like fragments in the  $^{238}\text{U} + ^{238}\text{U}$  reaction by four charge units to  $^{248}\text{Cm}$  and appropriately deplete the yields by  $I_n/I_f$ , the measured actinide cross sections in the  $^{238}\text{U} + ^{248}\text{Cm}$  reaction are reproduced. This shows that the energy distributions associated with a given (xp, xn)-transfer are the same in  $^{238}\text{U}$  collisions with  $^{238}\text{U}$  and  $^{248}\text{Cm}$ . Also, we find that an average of 3-4 neutrons are emitted from the primary fragments implying average excitation energies of 30-40 MeV in the heavy fragments that survived birth in both reactions. This again indicates that heavy actinide products are formed only in a small Q-value window located at low excitation energies<sup>2,3</sup>. Also shown in Fig. 1 are actinide yields from the  $^{48}\text{Ca} + ^{248}\text{Cm}$  reaction<sup>4</sup> at a comparable ratio  $E/B \approx 1.1$  which allows a meaningful comparison. The centroids  $\langle A \rangle$  of the isotopic distributions at fixed Z are at about the same value in both reactions. Slightly higher cross sections for  $^{98}\text{Cf}$  and  $^{99}\text{Es}$  isotopes result from the  $^{238}\text{U} + ^{248}\text{Cm}$  reaction. The  $^{100}\text{Fm}$  yields in the  $^{48}\text{Ca} + ^{248}\text{Cm}$  reaction are already significantly reduced as compared to the  $^{100}\text{Fm}$  yields in the  $^{238}\text{U} + ^{248}\text{Cm}$  reaction.  $^{101}\text{Md}$  could only be detected in bombardments of  $^{248}\text{Cm}$  targets with  $^{238}\text{U}$  projectiles. For  $^{259}\text{No}$  an upper cross section limit of 30 nb could be deduced. Apparently, for large mass transfers, reactions with  $^{238}\text{U}$  pro-

jectiles are better suited than those with  $^{48}\text{Ca}$  projectiles. In comparison with the  $^{238}\text{U} + ^{238}\text{U}$  reaction actinide cross sections from the  $^{238}\text{U} + ^{248}\text{Cm}$  reaction show an enhancement of about  $10^4$  for  $^{98}\text{Cf}$  and  $10^3$  for  $^{100}\text{Fm}$  products which is significantly higher than theoretically estimated.<sup>5</sup>

<sup>†</sup>Also at GSI Darmstadt

<sup>1</sup>J. V. Kratz, Paper presented at the Int. Conf. on Extreme States in Nuclear Systems, Dresden, Febr. 1980, GSI-Report 80-1; and M. Schädel et al. GSI Scientific Report 1979, GSI-Report 80-3, p. 63.

<sup>2</sup>M. Schädel et al., Phys. Rev. Lett. **41**, 469 (1978)

<sup>3</sup>M. Schädel, Proceedings of the Int. Conf. on Nuclear Physics, Berkeley, Aug. 1980, Vol. 1, p. 509,

<sup>4</sup>E. K. Hulet et al., Phys. Rev. Lett. **39**, 383 (1977)

<sup>5</sup>C. Riedel, W. Nörenberg, Z. Physik **A290**, 385 (1979)

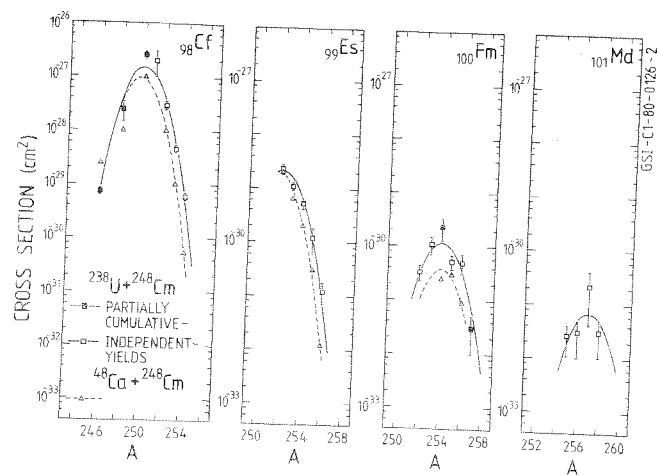


Fig. 1: Heavy actinide cross sections from the  $^{238}\text{U} + ^{248}\text{Cm}$  and  $^{48}\text{Ca} + ^{248}\text{Cm}$  (Ref. 4) reactions

Search for short-lived superheavy elements via fusion after instantaneous fission in the reaction of  $^{208}\text{Pb} + ^{238}\text{U}$

H. Gäggeler, W. Weber, G. Wirth  
 GSI Darmstadt

A search was made for superheavy elements (SHE) produced via a fast fission + fusion mechanism as proposed by Deubler et al.<sup>1</sup>. To explore the half-life region down to about 1 ms, the rotating wheel technique was used. This system was already used for the search for SHE in the U + U reaction.<sup>2</sup> In one experiment, rotating 11.4 mg/cm<sup>2</sup> uranium metal targets were bombarded with a 8.15 MeV/u  $^{208}\text{Pb}$  beam. The integral was  $5.7 \times 10^{15}$  particles which was accumulated within about 1 day. All reaction products emitted from the target in an emission cone of  $\pm 55^\circ$  (lab) were stopped in a stack of seven 8  $\mu\text{m}$  thick aluminium catcher foils which rotated with 80 revolutions per second. After end of bombardment, the catcher foils were exposed for one additional day to new Macrofol<sup>R</sup> foils in order to search also for longer lived species ( $h \leq T_{1/2} \leq d$ ). The fission tracks were then made visible by the spark technique.

A total amount of 817 tracks was detected within the Macrofol<sup>R</sup> foils which were exposed during bombardment. Two components were observed decaying with half-lives of about 1 ms and 14 ms, respectively (Fig. 1). These activities can most probably be assigned to the 0.9 and/or 1.0 ms  $^{240}\text{Am}^m$  and  $^{244}\text{Am}^m$  and to the 14 ms  $^{242}\text{Am}^m$  fission isomers. These nuclides are produced in the Pb + U reaction in damped collision processes. The mean production cross section for these spontaneously fissioning actinides are  $1.9 \times 10^{-32} \text{ cm}^2$  ( $^{240/244}\text{Am}^m$ ) and  $1.1 \times 10^{-32} \text{ cm}^2$  ( $^{242}\text{Am}^m$ ), respectively.

An analysis of the angular distribution of fission tracks within the catcher foils showed, that the observed nuclides were ejected from the target with high emission angles (e.g.  $\theta_{\text{lab}} = 55^\circ$  for the fission tracks of the first catcher foil). Sideward peaked distributions are typical for products from damped collision processes. SHE produced via a fission-fusion mechanism should be emitted from the target with low recoil energy ( $E < 100 \text{ MeV}^1$ ) and within a small emission cone ( $\theta_{\text{lab}} \leq 9 \text{ degree}^1$ ). Such nuclides, therefore, are expected to be stopped within the first and second catcher foil and should exhibit a forward peaked angular distribution. However, no such component was observed. Due to the detected Am fission isomers, only an upper limit for the production of fission-fusion like components can be obtained. This limit is defined by  $\leq 50$  fission tracks within the first and second aluminium catcher foil at a confidence level of 95%. During the one-day off-line exposure of the aluminium catcher foils to new Macrofol<sup>R</sup> foils no fission tracks were observed. The results extracted from these measurements are plotted as

a function of the assumed half-life of the SHE in Fig. 2 together with limits obtained from other experiments.<sup>3</sup>

<sup>1</sup>H.H. Deubler et al., Z. Physik A284, 237 (1978)

<sup>2</sup>H. Gäggeler et al., Phys. Rev. Lett. 45, 1824 (1980)

<sup>3</sup>T. Lund et al., submitted to Z. Physik

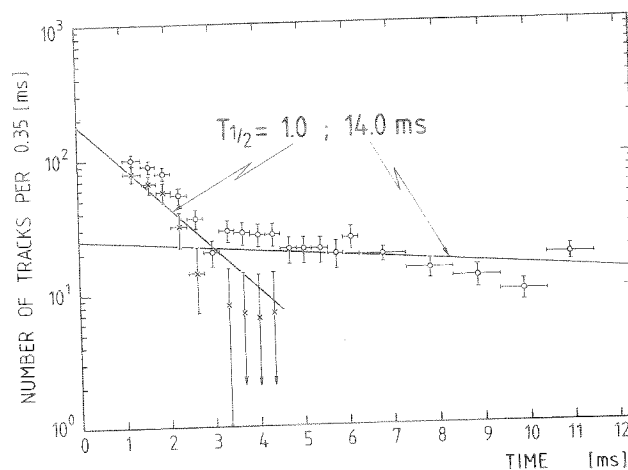


Fig. 1: Decay of the measured spontaneous-fission activity along one rotation of the foil stack.  
 circles: integral activity  
 crosses: difference between the measured values and the 14 ms component

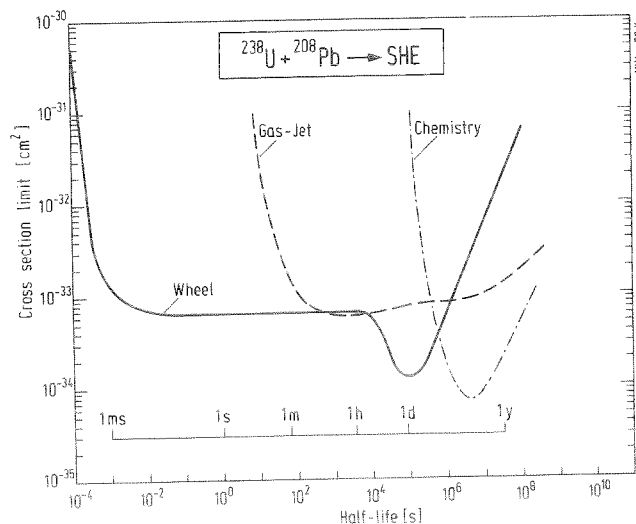


Fig. 2: Cross section limits for SHE from this work, "Wheel", together with data from the literature.<sup>3</sup>

No evidence for superheavy elements in the  $^{238}\text{U} + ^{248}\text{Cm}$  reaction

W. Bröchle, H. Gäggeler, J. V. Kratz, M. Schädel, K. Sümmerner, G. Wirth  
GSI Darmstadt

G. Herrmann, N. Trautmann, P. Peuser, G. Tittel,  
Institut für Kernchemie, Universität Mainz

E. K. Hulet, R. W. Lougheed  
Lawrence Livermore Laboratory, Livermore (USA)

J. M. Nitschke  
Lawrence Berkeley Laboratory, Berkeley (USA)

R. L. Hahn, R. L. Ferguson  
Oak Ridge National Laboratory, Oak Ridge (USA)

Following bombardment<sup>1</sup> of a  $7 \text{ mg/cm}^2$  thick metallic  $^{248}\text{Cm}$  target with  $3 \times 10^{15}$   $^{238}\text{U}$ -ions and chemical separations designed to isolate superheavy elements from the recoil catcher material and from the actinide elements the relevant chemical fractions mounted on thin carbon foils were counted for spontaneous fission activities in a fission-fragment-neutron multiplicity counter<sup>2</sup> for a total period of 440 days. The efficiency for detecting both fission fragments in coincidence is 58% and the efficiency for recording a single neutron is 32%. No fission events were recorded neither in a gas phase fraction (carrying elements that are volatile above room temperature up to  $1020^\circ\text{C}$ ) nor in a solution chemistry fraction (carrying elements forming strong bromide complexes). Elements that are volatile at or below room temperature (like Rn) were condensed on a copper cryostat faced by a single surface barrier detector. Here 2 events with energies of 60.6 MeV and 40.5 MeV were recorded within 86 days. Assuming 75% chemical yields for superheavy elements and 3 events or 6 events (compatible with 0 or 2 registered events at 95% confidence level) the cross section limits shown in Fig. 1 are obtained.

In addition to the off-line chemical recovery and search for superheavy elements, an on-line experiment was performed to detect gaseous species with half-lives of a minute or more. In this experiment products recoiling from the target were stopped in krypton gas. Gaseous products were swept together with the krypton gas through a set of filters and were then condensed upon a copper surface cooled to  $-150^\circ\text{C}$ . An annular surface barrier detector faced the cooled surface and continuously recorded  $\alpha$ - and spontaneous fission decay of the condensed products. Elements that are nonvolatile at room temperature were removed by the filters before reaching the Cu surface. No spontaneous fission events were detected.

The limits obtained in both these experiments are much less than optimum because of the premature failures of the  $^{248}\text{Cm}$ -metal targets.<sup>1</sup> Hence, the possibility

to produce superheavy elements with the deep-inelastic transfer mechanism has not been disproven inasmuch as the target limitations in these experiments did not allow a fair test. If these limitations can be overcome, the potential of the deep-inelastic transfer reaction to produce superheavy elements should be explored to the edge of our current limits of detection of about  $10^{-35} \text{ cm}^2$ .

<sup>1</sup>M. Schädel et al., GSI Scientific Report 1979, GSI 80-3, p. 63

<sup>2</sup>U. Tharun et al., GSI Scientific Report 1979, GSI 80-3, p. 165

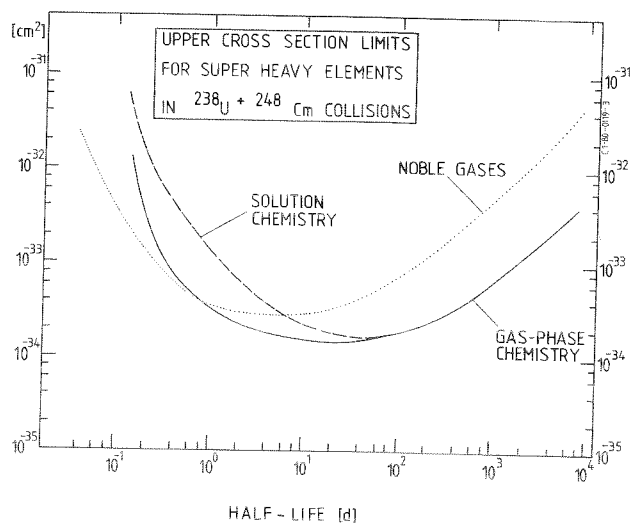


Fig. 1 Upper limits for the production cross section of spontaneously fissioning superheavy elements in the  $^{238}\text{U} + ^{248}\text{Cm}$  reaction as a function of the assumed half-life.



## Range Measurements of Uranium Projectiles in Solids

Y. Laichter, H. Geissel, M. Schädel, P. Armbruster  
GSI Darmstadt

A method has been developed for measuring the range and range straggling of  $^{238}\text{U}$  projectiles in solids. The uranium ions are implanted into a stack of foils. The concentration of the  $^{238}\text{U}$  atoms stuck in the individual foils is obtained by thermal neutron activation and then by measuring the gamma radiation activity of the  $^{239}\text{Np}$  radionuclide:



About  $5 \times 10^{12}$  uranium ions were implanted into a stack of foils at the UNILAC. The total thickness of the stack was larger than the expected range values of the measured 1.4 MeV/u ions in the given solid. Each of the individual foils was produced by evaporation at the GSI target laboratory and had a thickness of less than 5 % of the expected range.

After implantation the foils were cut out from their Al frames and pressed between two thin Polyethelene covers. These samples having an area of  $0.5 \text{ cm}^2$  each were irradiated by a total dose of  $\sim 5 \times 10^{16}$  thermal neutrons in the TRIGA reactor at Mainz. After a decay time of three days shortlived impurities had been decayed and then the samples were analyzed by a high resolution and high efficiency gamma spectrometer. For a given neutron dose, decay and counting time, the peak areas of the 106, 228, and 278 keV  $^{239}\text{Np}$  photopeaks are proportional to the number of  $^{238}\text{U}$  atoms in the samples.

In the figure we represent a number-distance curve obtained with a Ti stack. The peak areas are proportional to the number of  $^{238}\text{U}$  trajectories that succeeded to traverse the thickness  $x$  in the stack. On a probability paper a straight line is obtained, suggesting that the uranium range distribution in the stack is well defined by a Gaussian as already found for the ranges of  $^{252}\text{Cf}$  fission fragments<sup>3</sup>.

In the following table the measured mean range  $R_p$  and the longitudinal range straggling  $\sigma_{\parallel}$  in Ti are compared to the tabulated values<sup>1,2</sup>. The uncertainty given for  $R_p$  is determined mainly by the uncertainty of the  $\alpha$ -stopping cross sections used for the thickness determinations of the foils. The  $R_p$  value of Ref. 1 is higher by 14 % than the measured one. It was already reported<sup>4</sup> that in these tables the stopping powers of U in Ti are underestimated because  $Z_2$ -oscillations in the stopping powers were not taken into consideration.

<sup>1</sup>L.C. Northcliffe, R.F. Schilling, Nuclear Data Tables 7A, 233 (1970)

<sup>2</sup>V. Littmark, J.F. Ziegler, Vol. 6 of The Stopping and Ranges of Ions in Matter, Perg. Press (1980)

<sup>3</sup>Y. Laichter, N.H. Shafir, Nucl. Instr. and Meth. 177, 459 (1980)

<sup>4</sup>H. Geissel, P. Armbruster, K. Güttner, T. Kitahara, G. Kraft, GSI 79-11, p. 115

TABLE: Mean range  $R_p$  and range straggling  $\sigma_{\parallel}$  of 1.4 MeV/u  $^{238}\text{U}$  ions in Ti.

	measured	Ref. 1	Ref. 2
$R_p$ (mg/cm <sup>2</sup> )	$7.3 \pm 0.3$	8.3	$7.9 \pm 0.8$
$\sigma_{\parallel}$ (mg/cm <sup>2</sup> )	$0.47 \pm 0.15$	-	$0.25 \pm 0.05$

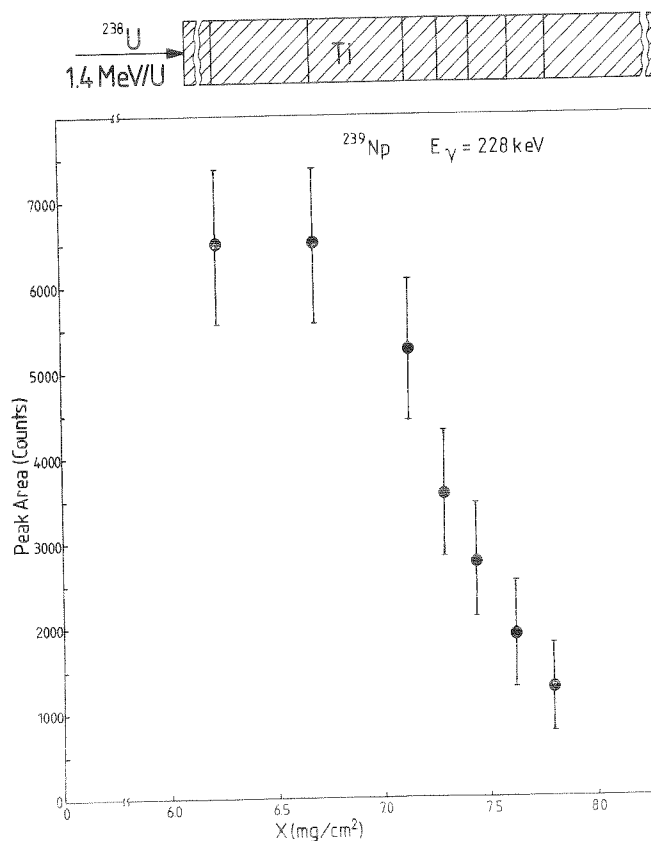


Fig.: Number-distance curve of 1.4 MeV/u  $^{238}\text{U}$  ions in Ti.

Preparation of  $^{248}\text{Cm}$  sources for experiments with heavy ions

N. Trautmann, R. Heimann, D. Gembalies-Datz, A.-K. Kaffrell,  
Institut für Kernchemie, Universität Mainz

$^{248}\text{Cm}$ -targets with varying thicknesses on different substrates are required for Coulomb excitation experiments<sup>1</sup>, Coulomb fission studies<sup>2</sup>, kinematic reaction studies in very heavy systems<sup>3</sup>, investigations on the positron production in heavy ion collisions<sup>4,5</sup>, and for the production of short-lived very heavy nuclei in transfer reactions<sup>6</sup>. For these collaborative experiments, limited amounts of  $^{248}\text{Cm}$  were made available by the US Department of Energy via LASL and ORNL in form of curium fluoride evaporated onto aluminum foils and on a glass cylinder, and as solutions in hydrochloric acid. In the latter case the activity was purified by absorption of  $^{248}\text{Cm}$  from 1 N HCl on a 'clean-up' cation exchange column and elution with 6 N HCl. The curium chloride was converted to the nitrate and molecularplated from isopropyl alcohol as will be described below. Evaporated  $\text{CmF}_3$  was dissolved in a mixture of 6 N HCl and  $\text{H}_3\text{BO}_3$  together with the Al foils and from the glass cylinder, then curium hydroxide was precipitated with NaOH and again dissolved in 1 N HCl. This solution was passed through an ion exchange column (300 x 6 mm; Dowex 50 x 8) and the curium was eluted with 6 N HCl. Half of the activity was converted to  $\text{CmF}_3$  for the preparation of thin  $^{248}\text{CmF}_3$  sources by vacuum evaporation, a method in which only a few percent are transferred to the collector foils whereas the bulk of the  $^{248}\text{Cm}$  is distributed over various parts of the evaporation set-up. For the production of further targets this bulk material was recovered and purified with the same procedure as used for the initial  $\text{CmF}_3$ . The other half of the isolated  $^{248}\text{Cm}$  was converted to the nitrate, dissolved in 0.2 N  $\text{HNO}_3$  and used in this form for electrodeposition. Aliquots of this solution (10-100  $\mu\text{l}$ ) were mixed with 5 ml isopropyl alcohol and filled in a molecularplating cell which is shown schematically in the Figure. A platinum wire served as the anode and a brass block as the cathode. The area to be plated, normally 6 mm in diameter, was confined by a conical teflon funnel. With a screw up the backing (Ti or Be) was fixed between cathode and solution container. A typical electrolysis, carried out with a current of 5 mA and a voltage of  $\sim 400$  V, lasted for about 45 min and resulted in deposition yields of

90-95 % for curium. After electrodeposition the samples were rinsed with isopropyl alcohol and then dried at 80 °C for 2 h. The yield was determined by  $\alpha$ -spectroscopy and by neutron-measurement with a  $^3\text{He}$ -counter. Several  $^{248}\text{Cm}$  targets with densities between 400  $\mu\text{g}/\text{cm}^2$  and 1.3  $\text{mg}/\text{cm}^2$  on titanium ( $\geq 0.6 \text{ mg}/\text{cm}^2$ ) and beryllium ( $\geq 1.85 \text{ mg}/\text{cm}^2$ ) substrates were prepared in this way.

<sup>1</sup>R.B. Piercey et al., submitted to Phys.Rev.Letters

<sup>2</sup>H. Backe et al., GSI Report 80-3, 4 (1980)

<sup>3</sup>Y. Civelekoglu et al., GSI Report 80-3, 30 (1980)

<sup>4</sup>H. Backe et al., GSI Report 80-3, 101 (1980)

<sup>5</sup>A. Balanda et al., GSI Report 80-3, 102 (1980)

<sup>6</sup>J.B. Wilhelmy et al., GSI Report 80-3, 178 (1980)

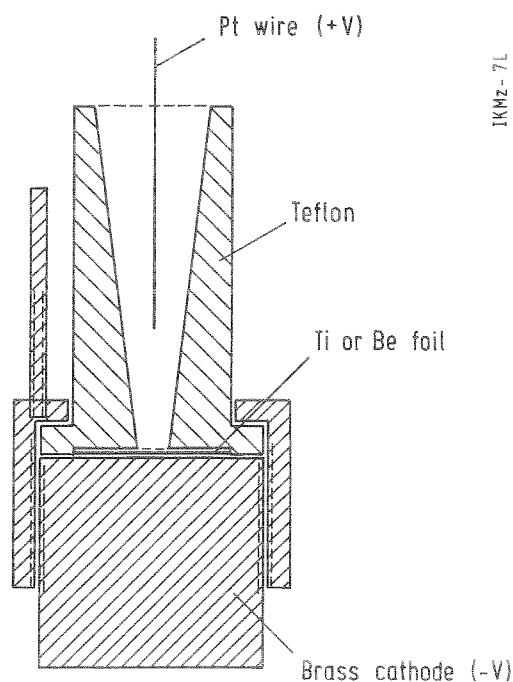


Fig.: Cell for the preparation of  $^{248}\text{Cm}$  targets by molecularplating

Tests of Curium Metal Targets for the Synthesis of Superheavy Elements\*

R.W. Lougheed, E.K. Hulet, R.L. Landingham  
Lawrence Livermore Laboratory

J.M. Nitschke  
Lawrence Berkeley Laboratory

H. Folger, J.V. Kratz, W. Bröchle, H. Gaggeler, I. Maor  
GSI Darmstadt

$^{248}\text{Cm}$  and Gd metal targets with densities up to  $7 \text{ mg/cm}^2$  on thin Ti, Mo, and Ta metal substrates were prepared for bombardment with  $7.5 \text{ MeV/u } ^{238}\text{U}$  ions. The  $^{248}\text{Cm}$  targets were prepared by in-situ reduction of curium sesquioxide with thorium metal and subsequent distillation of the Cm metal. Gd was used as an inactive substitute for Cm for testing purposes. Deposits of Gd metal withstood temperatures of  $1000^\circ\text{C}$  in DC electron bombardment tests over long periods, but failed<sup>1</sup> at  $\leq 3 \times 10^{15}$  particles of  $7.5 \text{ MeV/u } ^{238}\text{U}$  and at temperatures as low as  $170^\circ\text{C}$ .

Targets that had failed in 1979<sup>1</sup> and in additional tests in 1980 have been examined using scanning electron microscopy (SEM), microphotography, X-ray crystallography, and electron microprobe techniques to determine failure mechanisms. Metallurgical examination of destroyed targets indicated that most likely the failure mechanism was tensile stress caused essentially by the multiple temperature cycling of the targets in the pulsed heavy-ion beam. All targets (both Gd and Cm) failed in a similar fashion. Gradually, valleys of about 2 mm length formed in the targets. These valleys grew until a stress crack opened in the bottom (Fig. 1). The cracks were in the direction of the rolling lines in the substrate. No significant chemical reactions, alloying, melting or recrystallization were detected. The lack of recrystallization, even in a Mo-foil on which local melting of the Gd metal occurred ( $MP = 1312^\circ\text{C}$ ), indicated that the Gd reached temperatures several hundred degrees higher than the substrate. The apparent higher temperatures reached in the Gd vs. Mo layers do not agree with calculated heat transfer rates. This may indicate a large reduction in thermal conductivity or a problem in transferring heat across the Gd-Mo interface to the fast flowing  $\text{N}_2$  cooling gas on the Mo side. The large temperature difference between the Gd and the Mo layers caused considerable tensile stress. In addition the targets underwent about a million temperature cycles before failing which is beyond the stress-failure point of many metals. Heating and cooling rates during these cycles were thousands of degrees per second.

As a consequence of these results we have considered and partially tested several approaches for increasing the stress failure limits of the targets. These tests indicate that cracks also develop in Mo foils that were

annealed after rolling, as well as in Ta foils where rolling structures are optically not visible.

Also tests with pulsed electron beams were performed. These tests showed that the  $^{238}\text{U}$ -ion failure mechanisms cannot be duplicated. Thus, also other effects such as radiation damage, and penetration of the rare gas in the recoil chamber<sup>1</sup> into the Gd or Cm and subsequent expansion, have to be considered.

We plan to investigate the effect of equally cooling both sides of the target in the near future. One further possibility is to relax the crystal defects and stresses by periodical annealing before the targets fail. Both processes require a major redesign of the target system.

\*condensed from R.W. Lougheed et al., Report UCRL-84604 (1980), to be published in Nucl. Instr. and Meth.

<sup>1</sup>M. Schädel et al., GSI Scientific Report 1979, GSI 80-3 (1980), p. 63 and J.V. Kratz, Report GSI 80-1 (1980).

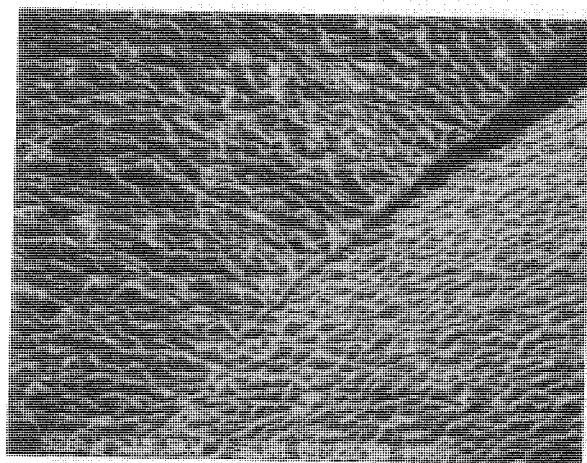


Fig. 1: SEM photograph of a destroyed Gd-Mo target from the Gd side. The irregular bumps develop during bombardment from flat, hexagonal grains of the unirradiated material.

On the separation of volatile superheavy elements from copper catchers

Wo Fan\* and H. Gäggeler  
GSI Darmstadt

Much efforts are presently made to search for superheavy elements (SHE) from damped reactions between  $^{238}\text{U} + ^{248}\text{Cm}$ .<sup>1</sup> In these experiments nuclear chemistry methods play a decisive role for the separation of long-lived SHE from the bulk of other reaction products. SHE around  $Z=114$  are predicted to be highly volatile, a fact which can be used for their separation in the gas phase. In the  $^{238}\text{U} + ^{248}\text{Cm}$  experiments reaction products recoiling from the target are stopped in a catcher placed behind the target. After bombardment, evaporation of the SHE from the catcher material can be achieved by heating it in a quartz apparatus in a carrier gas stream. As catcher material a Cu foil stack may be used.<sup>2</sup> In order to estimate appropriate thicknesses of the Cu foils, the diffusion coefficient  $D$  for SHE has to be estimated. This can be done by using the equation

$$D = D_0 \left( \exp - \frac{Q}{RT} \right), \text{ where}$$

$Q$ : activation energy of diffusion  
 $D_0$ : constant.

The value for  $Q$  can be obtained from the empirical relation<sup>2</sup>

$$\log(Q) = a \cdot \log[V_2 - 6(E_2 - E_1)] + b, \text{ where}$$

$V_2$ : atomic volume of the SHE  
 $E_2, E_1$ : electronegativities of SHE and Cu  
 $a, b$ : constants.

From a least-squares fit of known diffusion constants for elements in copper, average values for  $a, b$  and  $D_0$  may be deduced. Then, diffusion constants  $D$  for SHE in Cu can be obtained by extrapolation. Some estimated values for the activation energy  $Q$  and the constant  $D_0$  together with calculated values for the diffusion constant  $D$  at a temperature of  $1000^\circ\text{C}$  are given in the Table for the elements 112 to 116. These relatively high values for  $D$  ensure a quantitative release of these elements from thin Cu foils (thickness about  $10\ \mu\text{m}$ ) if heated up to  $1000^\circ\text{C}$  for  $\geq 1\ \text{h}$  as can be verified from the following equation<sup>2</sup>

$$F = 1 - \frac{8}{\pi^2} \exp\left(-\frac{Dt}{d^2}\right), \text{ where}$$

$F$ : release from a plate (foil)  
 $t$ : heating time in seconds  
 $d$ : foil thickness in cm.

After release, volatile species have to be purified, mainly from actinides, and to be deposited on thin foils for counting purposes. A very simple and effective technique is to use high-temperature quartz-filled columns which quantitatively adsorb actinides. In order to deduce the optimum transport temperature, the behaviour of  $^{212}\text{Pb}$  tracer was studied in quartz columns. This element behaves like the least volatile SHE<sup>3</sup>, i.e. represents the

most difficult element to be isolated and transported in a gaschromatographic system. The adsorption behaviour of a volatile species on a surface can be studied using thermochromatography. From measured adsorption temperatures ( $T_a$ ) at different values of the retention time ( $t_r$ ) and gas-flow velocity ( $v_0$ ), the thermodynamical properties adsorption enthalpy ( $\Delta H_a^0$ ) and entropy ( $\Delta S_a^0$ ) may be obtained.<sup>4</sup> In the Figure are plotted measured values of  $t_r v_0 / T_a$  versus  $1/T_a$  for  $^{212}\text{Pb}$  on quartz with  $\text{H}_2$  (crosses) and with the inert gas Ar (circles) as carrier gas. The adsorption values deduced from the plot show clearly that in the hydrogen system Pb can easily be transported in quartz due to the relatively low adsorption enthalpy of  $53\ \text{kcal/Mol}$  which presents evidence for a metallic behaviour. In the Ar system, however, the adsorption values are much increased indicating that chemical processes occur with the quartz surface which makes a quantitative and fast transport of Pb questionable.

<sup>1</sup>W. Bröchle et al., this report, p.

<sup>2</sup>T. Reetz et al., Radiochim. Acta, **24**, 69 (1977)

<sup>3</sup>B. Eichler, Kernenergie, **19**, 307 (1976)

<sup>4</sup>B. Eichler et al., Radiochim. Acta, **26**, 193 (1979)

Table Estimated values for  $Q$  and  $D_0$  and calculated diffusion constants for SHE in Cu at  $1000^\circ\text{C}$

element	$D_0 [\text{cm}^2\text{s}^{-1}]$	$Q [\text{kJMol}^{-1}]$	$\log D [\text{cm}^2\text{s}^{-1}]$
112	0.3	185	- 8.1
113	0.2	175	- 7.9
114	0.2	172	- 7.8
115	0.1	164	- 7.6
116	0.1	166	- 7.7

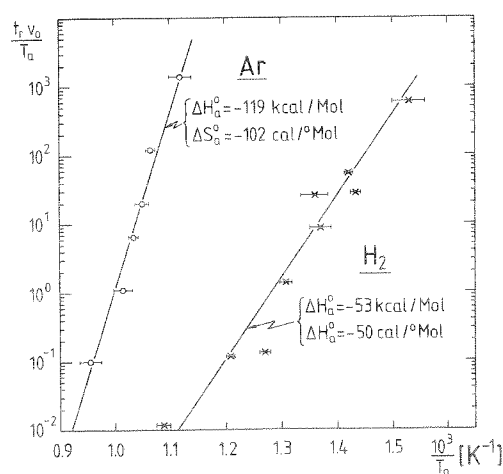


Figure: Retention data  $t_r v_0 / T_a$  for  $^{212}\text{Pb}$  on quartz as function of  $1/T_a$ . (see text)

## Separation of reaction products by vacuum thermochromatography

N. Greulich, U. Hickmann, N. Trautmann  
Institut für Kernchemie, Universität Mainz

The applicability of vacuum thermochromatography for the separation of nuclear reaction products was investigated with fission product mixtures at a pressure of about  $10^{-2}$  mbar. Due to the molecular flow pattern obtained at such a pressure this separation method should be much faster<sup>1</sup> than the thermochromatography under atmospheric conditions<sup>2</sup>.

A  $KCl/N_2$  gas-jet was used to transport the fission products, produced at the Mainz reactor, to a catcher consisting of a quartz wool plug. After a collection time of normally 15 min the quartz wool plug was placed in the first part of a quartz tube with an inner diameter of 3 mm. This part was kept at  $950^\circ C$  whereas a negative temperature gradient of  $18^\circ C/cm$  was established along the column. Within 10 s the thermochromatographic column was evacuated to  $4 \times 10^{-3}$  mbar. After a separation time of 15 min the element distribution was determined by measuring the activity along the column in 2 cm long sections with a shielded  $Ge(Li)$  detector. In some experiments a chlorinating agent was added in form of a second quartz wool plug wetted with thionylchloride and located in front of the catcher in the colder part of the column. Hereby the evacuation time was increased to 20 s and the pressure in the column to  $7 \times 10^{-3}$  mbar. The Table gives the deposition temperatures of the elements in the thermochromatographic column and in the

**Table:** Deposition temperatures in  $^\circ C$  of fission products under various experimental conditions

Element	$N_2$	Air	6,3 vol% $SOCl_2$	$SOCl_2$
	1,01 b	$4 \cdot 10^{-3}$ mb	1,01 b	$7 \cdot 10^{-3}$ mb
Rb, Cs	950	950, 720	830	550
Sr, Ba	950	950	920	920
Y, R.E.	950	950	920	830
Mo	950	-	900	160
Tc	530	630, ch.	90, ch.	480, 250, ch.
Sb	950	-	900	790
Te	710	650, 440	490	250
Br, I	230, ch.	ch.	20, ch.	ch.

ch. = charcoal trap at the end of the thermochromatographic column

connected charcoal trap which was kept at room temperature. Under reduced pressure ( $4 \times 10^{-3}$  mbar) most of the deposition zones are shifted to lower temperatures; the sequence of the elements remains unchanged. The efficiency of the volatilization increases with the halogenating agent  $SOCl_2$ .

In a series of experiments at a pressure of  $4 \times 10^{-3}$  mbar the separation time was varied between 2 and 45 min. In the Figure the deposition temperatures for tellurium and technetium are shown as a function of the separation time together with theoretical curves for different adsorption enthalpies calculated according to Ref.<sup>1</sup>. For the less volatile components of the elements tellurium and technetium adsorption enthalpies of 230 kJ/mol and 240 kJ/mol, respectively, can be estimated. The deposition behaviour of a second, more volatile species of these elements which moves with increasing separation time from the colder part of the column to the charcoal trap is not in agreement with constant adsorption enthalpies, however.

<sup>1</sup>B. Eichler, ZfK Rossendorf Report 346 (1977)

<sup>2</sup>U. Hickmann et al., Nucl.Instr.Meth. 174, 507 (1980)

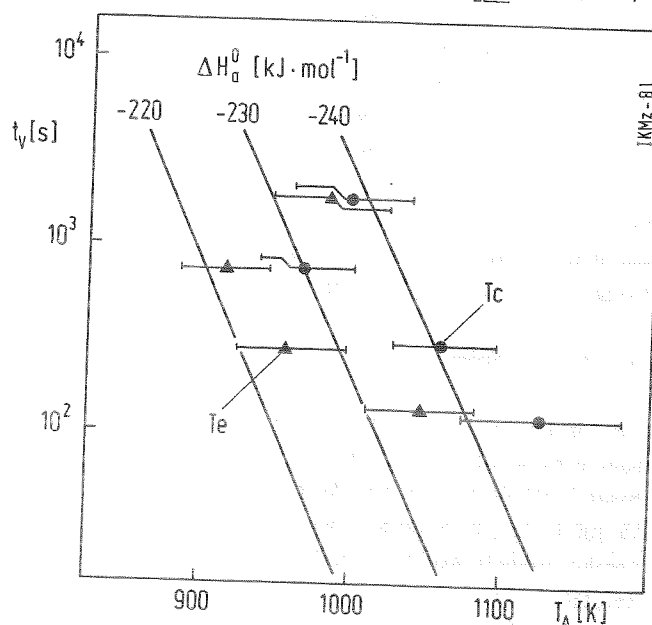


**Fig. 1:** Separation time  $t_v$  plotted against deposition temperature  $T_A$  for technetium and tellurium

Status report on the HELIOS system

A.K. Mazumdar, H. Wagner, W. Walcher  
FB Physik, Philipps-Universität Marburg

M. Brügger, N. Trautmann, W. Ziegert  
Institut für Kernchemie, Universität Mainz

An improved performance of the helium-jet on-line isotope separation facility HELIOS<sup>1</sup> has been achieved by technical modifications and by improvements in the operation of the gas-jet system and of the integrated skimmer ion source in the high temperature surface ionization (HTSI) and in the hollow cathode (HC) mode.

A more effective ion source power supply with an electron bombardment heating power up to 600 W was constructed and installed. The required stabilisation of the ion energy at an accelerating voltage of 25 kV for laser fluorescence measurements on neutron-rich fission products was obtained with a feed-back voltage stabilizer circuit resulting in an inhomogeneity of less than  $4 \times 10^{-5}$ .

The ionization efficiencies of 15-20 % measured<sup>2</sup> for alkaline earth and rare earth elements in the HTSI mode at an ionizer temperature of  $\sim 2700$  K (350 W electron bombardment power) could be increased by a factor of  $\sim 2$  at 500 W as shown in off-line experiments<sup>3</sup>. Further improvements are expected for an all-metal ion source equipped with two separate heating arrangements in order to reduce the cold surface area and to prevent condensation of the reaction products. First tests with this version are underway. As a first step of a study on the influence of the cluster materials on the ionization efficiency in a surface ion source several inorganic compounds with electron work functions between 4.3 eV (K) and 9.4 eV (Zn) were investigated with respect to their transport yield in the helium-jet. The Figure shows the transport efficiencies for  $ZnBr_2$ ,  $PbCl_2$  and  $MgCl_2$  together with that for KCl which has been used so far as cluster material. Corresponding ion source experiments with these cluster materials are not yet completed.

The relatively low skimmer transmission of  $\sim 20$  % may be traced back to the large angular divergence measured as  $20-30^\circ$  for size selected KCl clusters<sup>1</sup> which is in contradiction to previous measurements<sup>4</sup>. A two stage skimmer system taking into account the determined cluster distribution is under construction.

Using the ion source in the hollow cathode mode we have investigated the dependence of the ionization efficiency on the arc discharge power and on the pressure inside the ion source generated by varying the helium pressure in the target chamber and the distance between the end of the capillary and the skimmer. Under optimum conditions (high arc discharge power, low pressure) an enhancement by a factor of 3 compared to former measurements<sup>2</sup> was observed for antimony and tellurium. With argon as transport gas in the jet system instead of helium a lower effectivity of the hollow cathode ion source has been found caused by sputtering effects.

<sup>1</sup>A.K. Mazumdar et al., Nucl. Instr. Meth. **174**, 183 (1980)

<sup>2</sup>A.K. Mazumdar et al., Nucl. Instr. Meth., in press

<sup>3</sup>H. Danigel, private communication, 1979

<sup>4</sup>A.K. Mazumdar et al., Nucl. Instr. Meth. **139**, 319 (1976)

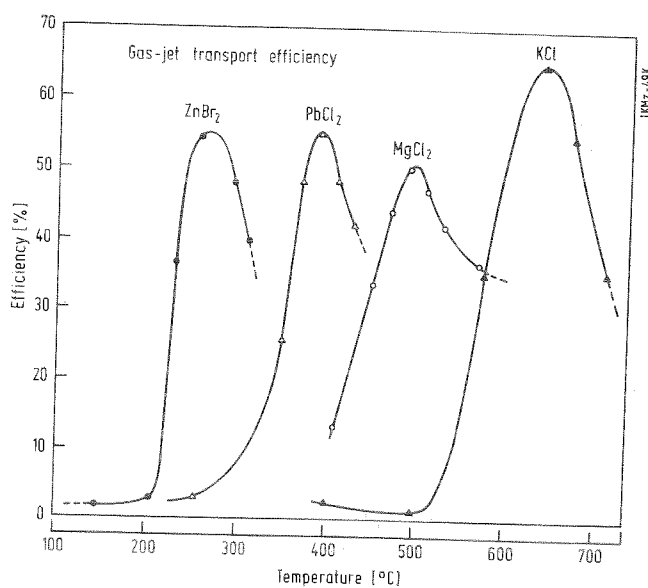


Fig.: Gas-jet transport efficiency for various inorganic cluster materials as a function of the oven temperature